

# An Improved Force Field for the Prediction of the Vapor–Liquid Equilibria for Carboxylic Acids

Ganesh Kamath, Feng Cao, and Jeffrey J. Potoff\*

Department of Chemical Engineering and Materials Science, Wayne State University, Detroit, Michigan 48202

Received: March 31, 2004; In Final Form: June 30, 2004

An improved united-atom force field, based on a Lennard-Jones plus point charge functional form, for carboxylic acids is proposed. Point charges are determined from a Mulliken population analysis of *ab initio* calculations performed at the MP2 level of theory with the 6-31+g(d,p) basis set. The Lennard-Jones well depth and size parameters for the carboxyl carbon interaction site were determined by fitting to single-component vapor–liquid equilibrium data for acetic acid, while the remaining Lennard-Jones parameters were taken from the TraPPE-UA force field. Histogram-reweighting Monte Carlo simulations in the grand canonical ensemble were used to determine the vapor–liquid coexistence curves, vapor pressures, and critical points predicted by the new force field. The new force field was found to describe accurately the phase equilibria of acetic acid, with mean unsigned errors in the saturated liquid density of less than 1.6%. The critical temperature and density predicted by the new force field were within 1% of experimental values. Additional calculations were performed in the grand canonical and Gibbs ensembles to determine the coexistence properties predicted by the optimized potentials for liquid simulations united-atom (OPLS-UA), all-atom (OPLS-AA), and CHARMM force fields. Simulations in the isobaric–isothermal ensemble were used to determine selected radial distribution functions predicted by the four force fields at 300 K and 1 bar.

## I. Introduction

In principle, the accuracy of molecular simulation is limited only by the intermolecular force field used to describe the interactions between molecules. Development of accurate force fields for carboxylic acids is of particular interest because the carboxyl functional group provides a self-assembling moiety in many molecules of technological and biological interest. Examples include the use of partially fluorinated fatty acids as drug delivery agents<sup>1–3</sup> and hexadecanoic acid as a template for the formation of nanoscale monolayer structures.<sup>4</sup>

While significant effort has occurred in the development of force fields for polar fluids such as alcohols<sup>5,6</sup> and water,<sup>7–13</sup> there has been relatively little activity in the development of accurate force fields for carboxylic acids. Existing force fields for acetic acid include the optimized potentials for liquid simulations united-atom (OPLS-UA)<sup>14</sup> and all-atom (OPLS-AA)<sup>15</sup> and CHARMM.<sup>16,17</sup> These force fields are similar in that they all utilize a Lennard-Jones plus fixed point charge functional form to model dispersive and Coulombic interactions. Recently, Chen and Siepmann used Aggregation Volume Bias Monte Carlo (AVB-MC) simulations in the Gibbs ensemble<sup>18</sup> to determine the vapor–liquid coexistence curve and heat of vaporization of acetic acid as predicted by the OPLS-UA force field. They found that the OPLS-UA force field predicts a critical temperature that is approximately 90 K higher than experiment. Significant deviations in the saturated vapor and liquid densities were also seen at elevated temperatures, while the saturated liquid density was found to be in close agreement with experiment only at 300 K. The vapor–liquid coexistence curves, vapor pressures, and critical points predicted by the OPLS-AA and CHARMM force fields have not yet been determined by simulation.

In this work, we develop a new united-atom force field for acetic acid that is parametrized specifically to yield accurate predictions of the vapor–liquid coexistence curve, vapor pressure, and critical point. This force field utilizes a Lennard-Jones plus fixed point charge functional form, similar to the OPLS and CHARMM force fields. *Ab initio* calculations are used to determine the necessary point charges for each pseudo-atom. In the parametrization of our force field, we take advantage of the transferability of parameters built into the TraPPE-UA atom force field. Parameters for the CH<sub>3</sub>, –OH, and =O units are taken directly from the TraPPE-UA force field.<sup>5,19,20</sup> The Lennard-Jones well depth and size for the carboxyl carbon remain the only adjustable parameters.

The specific details for each of the force fields studied in this work are given in the next section. In section 3, we provide the details of the grand canonical histogram-reweighting, Gibbs ensemble, and *NPT* Monte Carlo simulations used in this work. In section 4, the single component vapor–liquid coexistence curve, vapor pressures, and radial distribution functions are presented for the new force field as well as the OPLS-UA, OPLS-AA, and CHARMM force fields. The conclusions of this work can be found in section 5.

## II. Models

Nonbonded interactions for all of the force fields of interest in this work are described by pairwise additive Lennard-Jones 12-6 (LJ) potentials and Coulombic interactions of partial charges

$$U(r_{ij}) = 4\epsilon_{ij} \left[ \left( \frac{\sigma_{ij}}{r_{ij}} \right)^{12} - \left( \frac{\sigma_{ij}}{r_{ij}} \right)^6 \right] + \frac{q_i q_j}{4\pi\epsilon_0 r_{ij}} \quad (1)$$

where  $r_{ij}$ ,  $\epsilon_{ij}$ ,  $\sigma_{ij}$ ,  $q_i$ , and  $q_j$  are the separation, LJ well depth, LJ size, and partial charges, respectively, for the pair of interaction

\* To whom correspondence should be addressed. E-mail: jpotoff@chem1.eng.wayne.edu. Fax: 313 577 3810. Phone: 313 577 9357.

**TABLE 1: Parameters for Nonbonded Interactions Used in This Work. Letters in Parentheses Indicate the Atom a Particular Site Is Bonded To**

model	atom/group	$q_i$ (e)	$\sigma_{ii}$ (Å)	$\epsilon_{ii}/k_b$ (K)	1–4 $\sigma_{ii}$ (Å)	1–4 $\epsilon_{ii}/k_b$ (K)
new	C	0.42	3.90	41.0		
	O=(C)	−0.45	3.05	79.0		
	O−(H)	−0.46	3.02	93.0		
	H	0.37	0.0	0.0		
	CH <sub>3</sub> −(C=)	0.12	3.75	98.0		
	CH <sub>2</sub> −(C=)	0.12	3.95	46.0		
	(CH <sub>3</sub> )−CH <sub>2</sub> −(CH <sub>3</sub> )	0.0	3.95	46.0 [19]		
OPLS-UA	C	0.55	3.75	52.9		
	O=(C)	−0.50	2.96	105.7		
	O−(H)	−0.58	3.00	85.6		
	H	0.45	0.0	0.0		
	CH <sub>3</sub>	0.08	3.91	80.6		
OPLS-AA	H−(O)	0.45	0.000	0.000		
	O−(H)	−0.53	3.000	85.547		
	C=(O)	0.52	3.750	52.838		
	O=(C)	−0.44	2.960	105.675		
	C−(H)	−0.18	3.500	33.212		
	H−(C)	0.06	2.420	7.548		
CHARMM	H−(O)	0.44	0.4	23.148	0.4	23.148
	O−(H)	−0.61	3.154	76.539	3.154	23.148
	C=(O)	0.75	3.564	35.225	3.564	35.225
	O=(C)	−0.55	3.029	60.356	2.495	60.386
	C−(H)	−0.3	3.671	40.257	3.3385	5.032
	H−(C)	0.09	2.352	11.071	2.352	11.071

sites  $i$  and  $j$ . The nonbonded parameters for each of the force fields used in this work are listed in Table 1. Lorentz–Berthelot combining rules are used to determine cross-parameters for unlike Lennard-Jones interactions.<sup>21,22</sup>

For the OPLS-UA and new force field, these nonbonded interactions were only used for interactions of atoms or pseudoatoms belonging to different molecules or belonging to the same molecule but whose interactions are not accounted for by any of the intramolecular bonded potentials. In the OPLS-AA force field, Lennard-Jones interactions are also evaluated for intramolecular atom pairs separated by three or more bonds. These interactions are scaled by a factor of  $1/2$  to permit the use of the same well depth, size, and charge parameters for inter- and intramolecular interactions. The CHARMM force field does not use a general scaling rule for 1–4 interactions. Instead, specific Lennard-Jones parameters are used and listed in Table 1. In addition to 1–4 interactions, the CHARMM force field includes 1–3 interactions that utilize a quadratic functional form

$$U_{UB} = K_{UB}(S - S_0)^2 \quad (2)$$

where  $K_{UB}$  is the Urey–Bradley force constant, given in Table 4, and  $S$  is the Urey–Bradley 1,3 distance.

The OPLS-UA and new force fields utilize fixed bond lengths, which are listed in Table 2. These bond lengths were originally determined from experimental data.<sup>23</sup> The OPLS-AA and CHARMM force fields, on the other hand, allow for bond stretching and contraction. The energetics of bond stretching for the OPLS-AA and CHARMM force fields is given by

$$U_{bonds} = K_b(b - b_0)^2 \quad (3)$$

where  $K_b$  is the bond stretching constant,  $b$  is the measured bond length, and  $b_0$  is the equilibrium bond length. The values for the bonded parameters for the CHARMM and OPLS-AA force

**TABLE 2: Bond Lengths, Bond Angles, and Bending Constants for New and OPLS-UA Force Fields**

bond	length [Å]	bend	angle [deg]	$k_\theta/k_b$ [K rad <sup>−2</sup> ]
C=O	1.214	∠H–O–C	107	17600
C–O	1.364	∠O–C=O	123	40300
C–CH <sub>3</sub>	1.520	∠O–C–CH <sub>3</sub>	111	35300
O–H	0.970	∠O=C–CH <sub>3</sub>	126	40300

**TABLE 3: Bond Lengths, Bond Angles, and Bending Constants for the OPLS-AA and CHARMM Force Fields**

	bond	length [Å]	force constant [K Å <sup>−2</sup> ]	bend	angle [deg]	$k_\theta/k_b$ [K rad <sup>−2</sup> ]
OPLS-AA	O–H	0.945	278278.8	∠H–O–C	113	17612.6
	O–C	1.364	226447.5	∠O–C=O	121	40257.3
	C=O	1.229	286833.5	∠O–C–C	108	35225.2
	C–C	1.522	159519.7	∠C–C–H	109.5	17612.6
	C–H	1.09	171093.6	∠O=C–C	120.4	40257.3
CHARMM	O–H	0.96	274253.1	∠H–O–C	115	27676.9
	O–C	1.4	115739.8	∠O–C=O	123	25160.8
	C=O	1.22	377412.5	∠O–C–C	110.5	27676.3
	C–C	1.522	100643.3	∠C–C–H	109.5	16606.1
	C–H	1.111	162035.8	∠O=C–C	125.0	35225.2

**TABLE 4: Urey–Bradley Lengths and Force Constants for 1–3 Interactions Used in the CHARMM Force Field**

1–3 nonbonded <sup>a</sup>	UB length [Å]	force constant [K Å <sup>−2</sup> ]
O···O=(C)	2.2620	105675.5
(O)–C···H1	2.1630	15096.5
(H)–C···O	2.2620	105675.5
(H)–C···O=(C)	2.4220	10064.3
H1···H2	1.8020	2717.4
H2···H3	1.8020	2717.4
H1···H3	1.8020	2717.4

<sup>a</sup> The 1–3 interactions are indicated as “···”.

fields can be found in Table 3. In each of the force fields, a similar harmonic potential is used to control bond angle bending

$$U_{bend} = \frac{k_\theta}{2}(\theta - \theta_0)^2 \quad (4)$$

where  $\theta$  is the measured bond angle,  $\theta_0$  is the equilibrium bond angle, and  $k_\theta$  is the force constant. The equilibrium bond angles and force constants for the CHARMM and OPLS-AA force fields are listed in Table 3. For the new force field, values of the equilibrium bond angles and force constant were taken from the OPLS-UA force field and are listed in Table 2.

The motion of the dihedral angles about the carboxyl group for the OPLS-UA and new force field were governed by a cosine series

$$U_{torsion} = c_1[1 + \cos(\phi + f_1)] + c_2[1 - \cos(2\phi)] \quad (5)$$

with  $c_1/k_b = 630.0$  K and  $c_2/k_b = 1562.4$  K for both OCOH and CCOH interactions, but  $f_1 = 180^\circ$  for OCOH and  $f_1 = 0^\circ$  for CCOH. The dihedral angles for the alkane tails of pentanoic and octanoic acid were controlled by the OPLS-UA torsional potential.<sup>24</sup> The following functional form was used to control the rotation of pseudoatoms about their dihedral angles for all interactions in the OPLS-AA force field:

$$U_{torsion} = \frac{V_1}{2}(1 + \cos(\phi)) + \frac{V_2}{2}(1 - \cos(2\phi)) + \frac{V_3}{2}(1 + \cos(3\phi)) \quad (6)$$

**TABLE 5: Torsional Parameters for OPLS-AA and CHARMM Force Fields**

	dihedral	$k_\chi$	$n$	$\chi$	$\delta$
CHARMM	H—O—C=O	1031.6	1	2.0	$\pi$
	H—O—C—C	1031.6	1	2.0	$\pi$
	dihedral	$V_1$	$V_2$	$V_3$	
OPLS-AA	H—O—C=O	0.0	1383.8	0.0	
	H—O—C—C	377.4	1383.8	0.0	

The values of  $V_1$ ,  $V_2$ , and  $V_3$  used in this work are given in Table 5. For the CHARMM force field, the torsional potential is given by

$$U_{\text{torsion}} = k_\chi(1 + \cos(n\chi - \delta)) \quad (7)$$

where  $\chi$  is the dihedral angle. The values for  $n$ ,  $\delta$ , and the force constant used in this work are listed in Table 5.

**A. Force Field Development.** In the parametrization of our force field, we take advantage of the transferability of parameters built into the TraPPE-UA atom force field. Parameters for the  $\text{CH}_3$ ,  $\text{CH}_2$ , OH, and  $=\text{O}$  units are taken directly from the TraPPE-UA force field.<sup>5,19,20</sup> This leaves the Lennard-Jones well depth and size parameters for the carboxyl carbon as the only adjustable parameters for a given set of partial charges. Our original attempts to use partial charges from the OPLS-UA force field in our new force field failed. Many sets of Lennard-Jones parameters were tested; each parameter set overpredicted the critical temperature of acetic acid. A new set of partial charges was derived from a Mulliken population analysis of ab initio calculations utilizing MP2 theory and the 6-31+g(d,p) basis set. These calculations were performed with the Gaussian 98 software package.<sup>25</sup> Given this new set of partial charges, we were able to optimize the Lennard-Jones parameters for the carboxyl carbon such that a good representation of the experimental vapor–liquid coexistence curve, vapor pressure, and critical parameters was obtained.

### III. Simulation Details

**A. Grand Canonical Monte Carlo.** Grand canonical histogram-reweighting Monte Carlo simulations<sup>26,27</sup> were used to determine the vapor–liquid coexistence curves and vapor pressures for acetic, pentanoic, and octanoic acid as predicted by the new force field. The insertion of molecules in the GCMC simulations were enhanced through multiple first bead insertions<sup>28</sup> and the application of the coupled–decoupled configurational-bias Monte Carlo method.<sup>29</sup> Near the critical temperature, a minimum of 12 trial positions were used in the insertion of the first “bead” of the molecule, while a minimum of 10 trial positions are used for subsequent interacting sites. At lower temperatures, more trial positions were required to maintain adequate sampling of configuration space. To further enhance sampling in the vapor phase, aggregation volume bias Monte Carlo (AVBMC) was used.<sup>18</sup> The AVBMC method was not found to improve the sampling of liquid-phase configurations. The fractions of the various moves for each simulation were set to 15% for particle displacements, 15% for rotations, 35% for configurational bias regrowths, and 35% for insertions and deletions. Simulations were performed for a system size of  $L = 30$  Å. Lennard-Jones interactions were truncated at  $L = 14$  Å, and standard long-range corrections were applied.<sup>30</sup> An Ewald sum with tinfoil boundary conditions ( $\kappa L = 5$  and  $K_{\text{max}} = 5$ ) was used to calculate the long-range electrostatic interactions.<sup>31</sup> Simulations were equilibrated for 1 million Monte Carlo steps before run statistics were recorded, while production

runs were 50 million MCS. For each molecule of interest, 10 simulations were required to cover the temperature region  $T = 300$ –650 K. The histogram data resulting from these simulations were combined according to the multiple histogram method of Ferrenberg and Swendsen.<sup>32</sup> Over the course of each simulation, the number of molecules  $N$  and energy  $E$  were stored in the form of a list, which was updated every 250 MCS. The necessary probability distributions were extracted from this list after the completion of the simulation.

**B. Gibbs Ensemble Monte Carlo.** Monte Carlo simulations in the Gibbs ensemble<sup>33–36</sup> were used to determine the vapor–liquid coexistence curve, vapor pressures, and critical parameters of acetic acid predicted by the OPLS-AA and CHARMM force fields. A system size of 250 molecules was used for all calculations. Simulations were equilibrated for 20 million Monte Carlo steps before run statistics were recorded. Run statistics were collected for an additional 15 million Monte Carlo steps after completion of the equilibration period. As in the case of the grand canonical Monte Carlo simulations, the sampling of phase space was enhanced through the extensive use of the coupled–decoupled configurational-bias method.<sup>29</sup> The ratio of moves for each simulation were 2% volume exchange, 30% particle displacements, 18% configurational bias regrowths, 20% swap moves, and 30% rigid rotations. An Ewald sum with tinfoil boundary conditions ( $\kappa L = 5.6$  and  $K_{\text{max}} = 5$ ) was used to calculate the long-range electrostatic interactions.<sup>31</sup> Lennard-Jones interactions are truncated at  $L = 10$  Å, and standard long-range corrections are applied.<sup>30</sup>

**C. Isobaric–Isothermal Monte Carlo.** Monte Carlo simulations in the isobaric–isothermal ensemble were used to investigate the structural properties of acetic acid at 300 K and 1 bar for the OPLS-UA, OPLS-AA, CHARMM, and new force fields. For the united-atom force fields, simulations were performed for a system size of 500 molecules, while a system size of 250 molecules was used for the all-atom force fields. A smaller system size was used for the all-atom force fields to reduce the computational time necessary for the simulations. An equilibration period of 1 million Monte Carlo steps was used, after which run statistics were recorded for an additional 20 million MCS. The ratio of moves was 1% volume changes, 14% configurational bias regrowths, 70% translations, and 15% molecule rotations. Lennard-Jones interactions were truncated at  $L = 14$  Å and standard long-range corrections were applied.<sup>30</sup> An Ewald sum with the same parameters as used in the GCMC simulations was used to determine the long-range electrostatic interactions.

### IV. Results and Discussion

**A. Vapor–Liquid Coexistence of Acetic Acid.** The results of our Monte Carlo simulations for the vapor–liquid coexistence curves predicted by the OPLS-UA, OPLS-AA, CHARMM, and new force fields are shown in Figure 1. Selected values for saturated vapor and liquid densities and vapor pressures are listed in Table 6. The new force field yields saturated liquid densities that are in close agreement with experiment, with average deviations of approximately 1.6%. Saturated vapor densities are also in good agreement with experiment. The critical temperature and density for the new force field were determined by fitting the density scaling law and law of rectilinear diameters to subcritical coexistence data.<sup>37,38</sup> More accurate estimates of the critical parameters are possible through the use of mixed-field finite-size scaling methods.<sup>39</sup> In this case, however, the approximate nature of the force fields studied does not justify the added computational expense. For the new force field, we found  $T_c = 600.26$  K and  $\rho_c = 344.42$  kg/m<sup>3</sup>, which



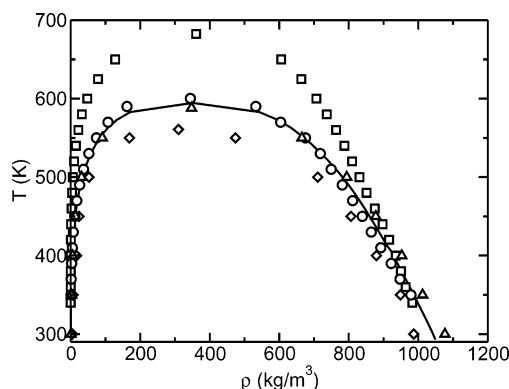


**Figure 1.** Vapor–liquid coexistence curves for acetic acid. Experimental data<sup>40</sup> and simulation results are shown as lines and symbols, respectively: new (circle), OPLS-UA (square), OPLS-AA (triangle), and CHARMM (diamond).

**TABLE 6: Selected Coexistence Points Predicted by Simulation for the New, OPLS-UA, OPLS-AA, and CHARMM Force Fields**

model	$T$ (K)	$P$ (bar)	$\rho_{\text{gas}}$ (kg/m <sup>3</sup> )	$\rho_{\text{liq}}$ (kg/m <sup>3</sup> )
new force field	550	38.84	74.96	676.96
	500	17.94	31.46	765.07
	450	6.786	12.35	844.77
	400	1.914	4.64	913.72
	350	0.341	1.28	967.33
OPLS-UA	650	57.30	127.97	605.60
	600	26.56	47.40	706.77
	550	10.87	18.00	775.64
	500	3.67	6.13	830.78
	450	0.93	1.64	886.71
	400	0.15	0.29	934.71
	350	0.02	0.028	970.85
OPLS-AA	300	0.001	0.00012	1020.62
	550	42.2	91.11	664.91
	500	20.9	31.189	794.02
	400	2.31	5.721	952.22
	350	1.48	2.337	1012.1
CHARMM	300	0.42	1.018	1076.4
	550	55.84	169.11	474.11
	500	23.50	52.90	710.35
	400	6.265	16.83	879.26
	350	1.941	6.705	948.41
	300	0.341	5.174	986.76

are in close agreement with the experimental values of  $T_c^{\text{exp}} = 594.6$  and  $\rho_c^{\text{exp}} = 350.6$  kg/m<sup>3</sup>.<sup>40</sup> The saturated liquid density predicted by the OPLS-UA force field at 300 K is in good agreement with experiment, which is as expected because the OPLS-UA force field was originally fit to reproduced liquid densities at 298 and 373 K. However, at higher temperatures the predicted saturated liquid densities are significantly too high and in error by as much as 20% as the critical point is approached. In addition, the OPLS-UA force field overpredicts the critical temperature by approximately 90 K. These results are consistent with the previous work of Chen and Siepmann.<sup>18</sup>

While the results of the OPLS-UA force field were disappointing, much better agreement with experimental vapor–liquid equilibrium data is achieved with the OPLS-AA force field. For this force field, saturated liquid densities are overpredicted slightly, deviating from experiment by approximately 3.5%. Fitting coexistence data to scaling laws yields results in a predicted critical temperature and density of  $T_c = 588.06$  K and  $\rho_c = 347.64$  kg/m<sup>3</sup>. Simulations of the CHARMM force field gave saturated liquid densities that were approximately 5% lower than experiment over the entire phase diagram. Saturated vapor densities are overpredicted by 35%. The critical

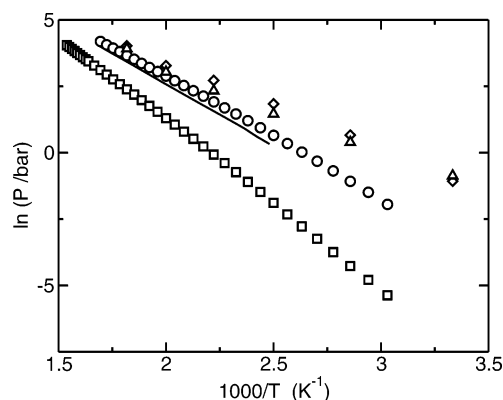


**Figure 2.** Clausius–Clapeyron plots of the saturated vapor pressure against inverse temperature for acetic acid. Experimental data<sup>40</sup> and simulation results are shown as lines and symbols, respectively: new (circle), OPLS-UA (square), OPLS-AA (triangle), and CHARMM (diamond).

**TABLE 7: Comparison of Estimated Normal Boiling Points and Critical Properties of Acetic Acid Predicted by the New, OPLS-UA, OPLS-AA, and CHARMM Force Fields**

	$T_b$ (K)	$T_c$ (K)	$\rho_c$ (kg/m <sup>3</sup> )	$P_c$ (bar)
experiment	391.2	594.6	350.6	58.0
new force field	379.8	600.26	344.42	65.74
OPLS-UA	450.6	682.39	360.62	97.29
OPLS-AA	330.2	588.06	347.64	40.4
CHARMM	320.1	560.72	310.13	57.2

temperature and density predicted by the CHARMM force field were  $T_c = 560.72$  K and  $\rho_c = 310.13$  kg/m<sup>3</sup>. Considering that vapor–liquid equilibrium data were not used in the original parametrization of the OPLS-AA and CHARMM force fields, the degree of agreement between simulation and experiment is remarkable.

The Clausius–Clapeyron plots used to determine the critical pressures and normal boiling points are shown in Figure 2. The normal boiling points and critical properties predicted by each force field are listed in Table 7. The new force field predicts a normal boiling point for acetic acid of  $T_b = 379.8$  K, which is the best prediction of the group of force fields studied in this work, but is still 11.2 K lower than experiment.<sup>40</sup> The new force field also gave the best prediction of the critical pressure of acetic acid  $P_c = 65.74$  bar, compared to the experimental value of 58.0 bar.<sup>40</sup>

The new force field predicted vapor pressures at low temperatures ( $T = 400$  K), shown in Figure 2, that were approximately 50% higher than experiment. This difference improved consistently as temperature increased. At  $T = 580$  K, the new force field gave vapor pressures that were only 20% higher than experiment. Part of this deviation has to do with the original parametrization of the various functional groups in the TraPPE-UA force field. Both the alkane and alcohol force fields from which our acetic acid force field was constructed were found to overpredict the vapor pressures when compared to experiment.<sup>5,19</sup>

For Lennard-Jones diatomics, it has been demonstrated that the slope of the Clausius–Clapeyron plot is affected by the aspect ratio of the molecule  $L^* = L/\sigma$ , where  $L$  is distance between site centers and  $\sigma$  is the collision diameter.<sup>41</sup> This phenomena has been exploited by others in the development of realistic intermolecular force fields for alkanes that offer improved predictions of the vapor pressure compared to the TraPPE-UA force field. Methods for altering the anisotropy of the molecule include the use of an explicit hydrogen representa-

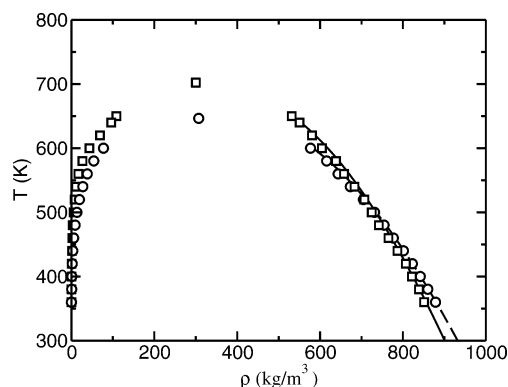


**Figure 3.** Vapor–liquid coexistence curves for pentanoic acid and octanoic acid. Pentanoic acid: simulation (circle), correlation of Daubert (solid line). Octanoic acid: simulation (squares), correlation of Daubert (dashed line).<sup>47</sup>

tion (TraPPE-EH),<sup>42</sup> alteration of the bond lengths between psuedoatom centers (Gibbs-99),<sup>43</sup> altering the effective molecule length by changing  $\sigma$  for certain pseudoatoms (NERD),<sup>44</sup> and anisotropic potentials (AUA).<sup>45</sup>

The situation for carboxylic acids, as well as ketones and other branched molecules, is complicated by the fact that there are two aspect ratios that must be considered, as opposed to one for alkanes. In this work, our goal was to develop the “best” force field for thermophysical property prediction within the restrictions of the TraPPE-UA scheme. Given only two free parameters,  $\epsilon_C$  and  $\sigma_C$ , the overall size of the molecule was fixed. Therefore, fitting to get the correct saturated liquid densities and critical temperature effectively fixes the vapor pressure. Adoption of an explicit hydrogen representation for the  $\text{CH}_3$  group, adding a Lennard-Jones interaction to the hydroxyl hydrogen, and treating the  $\epsilon$  and  $\sigma$  parameters for the carbonyl oxygen as additional free parameters would provide avenues for alteration of the molecule size (aspect ratio) and an improvement in the vapor pressure prediction.

Vapor pressures predicted by the OPLS-UA, OPLS-AA, and CHARMM force fields also show deviations from experiment. The OPLS-UA force field predicted vapor pressures that were significantly lower than experiment. At  $T = 540$  K, the OPLS-UA force field predicted vapor pressures that were a factor of 3.2 times lower than experiment. The error grew to a factor of 9 at  $T = 400$  K. These errors are primarily the result of a severe overprediction of the critical temperature, which shifted the entire pressure versus temperature curve to higher temperatures. The OPLS-AA force field yielded vapor pressures that were slightly higher than those predicted by the new force field and were approximately 60% higher than experiment. The CHARMM force field also significantly overpredicts the vapor pressure of acetic acid. At  $T = 400$  K, the vapor pressure predicted by the CHARMM force field was a factor of 6 higher than experiment. At  $T = 550$  K, this deviation was reduced to a factor of 1.8.

To demonstrate the transferability of the new force field, simulations were performed for pentanoic and octanoic acid. The vapor–liquid coexistence curves predicted by the new force field are shown in Figure 3 and compared to a correlation for the saturated liquid density given by<sup>47</sup>

$$\rho = A/B^{(1+(1-T/C)D)} \quad (8)$$

where  $A$ ,  $B$ ,  $C$ , and  $D$  are constants fit to reproduce the limited amount of experimental data and the units of  $\rho$  are  $\text{kmol/m}^3$ . The parameters used in eq 8 can be found in Table 9. Selected points from Figure 3 are listed in Table 8. The predictions of

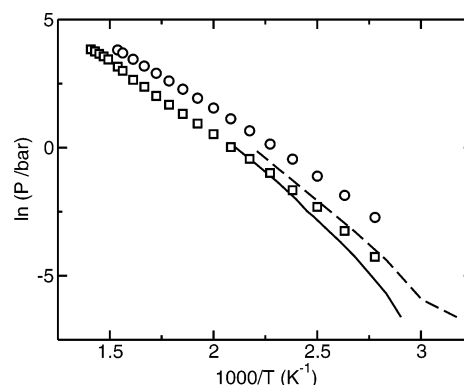


**Figure 4.** Clausius–Clapeyron plots of the saturated vapor pressure against inverse temperature for pentanoic acid and octanoic acid. Experimental data for pentanoic and octanoic acid are denoted by dashed lines and solid lines, respectively.<sup>48</sup> Predictions of the new force field are denoted by symbols: pentanoic acid (circle) and octanoic acid (square).

**TABLE 8: Selected Coexistence Points Predicted by the New Force Field for Pentanoic and Octanoic Acids**

	$T$ (K)	$P$ (bar)	$\rho_{\text{gas}}$ ( $\text{kg/m}^3$ )	$\rho_{\text{liq}}$ ( $\text{kg/m}^3$ )
pentanoic acid	600	24.21	77.13	576.97
	550	13.54	32.90	651.1
	500	4.72	13.16	731.33
	450	1.93	4.08	786.50
	400	0.33	1.04	841.76
octanoic acid	650	23.71	108.48	531.51
	600	9.74	43.37	604.46
	550	3.94	13.35	639.79
	500	1.54	5.06	724.72
	450	0.46	1.14	770.81
	400	0.15	0.27	821.70

**TABLE 9: Parameters for Predicting Saturated Liquid Density (Eq 8)**

	$A$	$B$	$C$	$D$
pentanoic acid	0.7853	0.26363	651.0	0.28151
octanoic acid	0.54070	0.26676	692.0	0.2802

the new force field for the saturated liquid densities for both pentanoic and octanoic acid are in excellent agreement with experiment and the correlation, demonstrating the transferability of the force field.

In Figure 4, the saturated vapor pressure for pentanoic and octanoic acid is presented in the form of Clausius–Clapeyron plots. The new force field was found to overpredict the vapor pressure of pentanoic acid by a factor of 2.6 at 400 K, with the relative error increasing with decreasing temperature. It should be noted that the kink in the experimental data for pentanoic acid is likely an error and does not have any special physical significance. The new force field predicts vapor pressures for octanoic acid that are in close agreement with experimental data<sup>48</sup> at 400 K. These results suggest possible inconsistencies in the experimental data, which were originally published in 1947.

Normal boiling points were extracted for pentanoic and octanoic acid from the Clausius–Clapeyron plots, Figure 4. For pentanoic acid,  $T_b^{\text{sim}} = 435.7$  K, which is lower than the experimental value of  $T_b^{\text{exp}} = 458.65$  K.<sup>49</sup> In the case of octanoic acid, the new force field predicted  $T_b^{\text{sim}} = 479.8$  K, which is approximately 7% lower than the predicted value of  $T_b^{\text{exp}} = 513$  K.<sup>47</sup>

Critical properties, such as temperature, density, and pressure, were determined by fitting coexistence data to scaling laws and through extrapolation of the Clausius–Clapeyron plots.

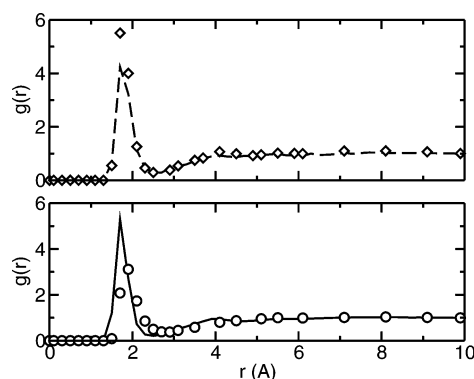


**Figure 5.** Radial distribution function of carboxyl oxygen–hydroxyl hydrogen in acetic acid. Top plot: CHARMM (diamond), OPLS-AA (dashed line). Bottom plot: new (circles), OPLS-UA (solid line).

The critical temperature for pentanoic and octanoic acid was determined to be 646.4 and 702.24 K, respectively. For pentanoic acid, our results are within 1% of the experimental value of  $T_c^{\text{exp}} = 639.9$  K.<sup>49</sup> In the case of octanoic acid, experimental data do not exist. Instead, we compare the predictions of simulation with the critical temperature<sup>47</sup> estimated by the Lydersen method<sup>50,51</sup> and find excellent agreement. The critical densities for pentanoic and octanoic acid predicted by the new force field were 307.05 and 300.12 kg/m<sup>3</sup>, respectively. We were unable to locate experimental data for comparison. The critical pressure of pentanoic acid was found to be 52.3 bar, compared to the experimental value of 36.3 bar.<sup>49</sup> The critical pressure of octanoic acid was determined to be 45.21 bar. As in the case of the other critical properties of octanoic acid, no experimental data were available for comparison.

**B. Structure of Acetic Acid.** The site–site radial distributions were calculated for each of the force fields from isobaric–isothermal simulations at 1 bar and 300 K. The hydroxyl hydrogen–carboxyl oxygen radial distribution function is shown in Figure 5. All of the force fields display a strong peak at approximately 1.8 Å, which is consistent with neutron scattering data.<sup>52</sup> The OPLS-UA and CHARMM force fields show similar behavior, and display the largest peaks. The OPLS-AA force field shows a slightly weaker peak at 1.8 Å. The new force field developed in this work, while also showing a degree of hydrogen bonding, has a significantly smaller peak than the other force fields studied. A comparison of the partial charges for the hydrogen in –OH and the oxygen in >C=O for each force field shows that the new force field has the smallest charges of the four force fields. Since partial charges are the only means of specifying associating type interactions, it is not a surprise that the new force field predicts less association than the OPLS-UA, OPLS-AA, or CHARMM force fields.

Acetic acid, with its two oxygen atoms, has two possible sites that can act as hydrogen bond acceptors. In Figure 6, the hydroxyl hydrogen–hydroxyl oxygen radial distribution is shown. The OPLS-UA, OPLS-AA, and CHARMM force fields show a small peak of similar magnitude at approximately 1.9 Å. The new force field shows a plateau starting at 1.9 Å. This suggests that while hydrogen bonding is possible between hydroxyl groups, it occurs with much less frequency than

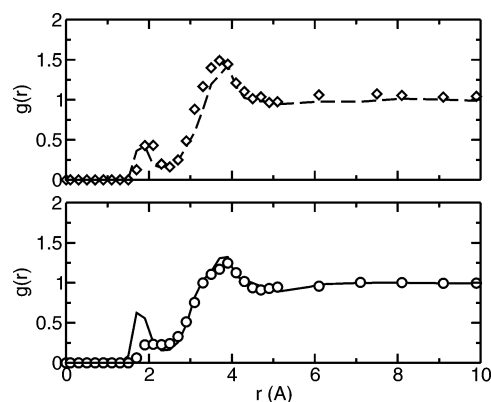


**Figure 6.** Radial distribution function of hydroxyl oxygen–hydroxyl hydrogen in acetic acid. Top plot: CHARMM (diamond), OPLS-AA (dashed line). Bottom plot: new (circles), OPLS-UA (solid line).

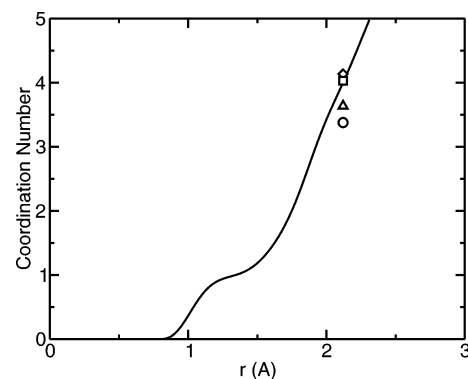


**Figure 7.** Hydroxyl hydrogen coordination number. Simulation results are shown as symbols: new force field (circle), OPLS-UA (square), CHARMM (diamond), OPLS-AA (triangle). The running coordination number obtained from neutron scattering experiments is shown as a solid line.

between –OH and >C=O groups. Compared to simulations of the TraPPE<sup>5</sup> and OPLS-UA<sup>46</sup> force fields for primary alcohols, hydrogen bonding between hydroxyl units in acetic acid is greatly reduced. This is because of steric hindrance created by the >C=O group that is not present in alcohols and the reduced partial charge placed on the hydroxyl oxygen. All of the force fields show very similar behavior for larger separations. The peak at 3.9 Å corresponds to the formation of dimers, with a hydrogen bond forming between the hydrogen in –OH and the oxygen in >C=O.

Finally, we investigated the coordination number for the hydroxyl hydrogen, which is defined as the number of atomic sites within a certain radius from the atom of interest. In Figure 7, we present preliminary neutron scattering data for the hydroxyl hydrogen coordination number<sup>53</sup> and compare these results to simulation. Due to the large size of acetic acid and the isotopic substitution method used, it was not possible to separate the inter- and intramolecular components that compose the coordination number. In particular, the intermolecular hydrogen bonding distance of 1.8 Å is the same as the intramolecular distance between the hydroxyl hydrogen and the carbonyl carbon. As a result, the coordination number

**TABLE 10: Predicted Boiling Point and Critical Properties of Pentanoic and Octanoic Acid**

		$T_b$ (K)	$T_c$ (K)	$\rho_c$ (kg/m <sup>3</sup> )	$P_c$ (bar)
pentanoic acid	new force field	435.7	646.4	307.05	52.3
	correlation/exp	458.65 [ref 47]	639.9 [ref 49]	N/A	36.3 [ref 49]
octanoic acid	new force field	479.8	702.24	300.12	45.21
	correlation	513.05 [ref 47]	692 [ref 47]	N/A	N/A



presented includes both inter- and intramolecular interactions. Experimental data show that there are exactly four atoms within a radius of 2.12 Å from the hydroxyl hydrogen, which suggests a planar dimer structure. We note, however, that other structures are possible and in our simulations we have also found significant fractions of trimer, tetramer, and pentamer aggregates. All of the force fields show reasonable agreement with experimental data, with the OPLS-UA and CHARMM force fields in closest agreement, predicting coordination numbers of 4.03 and 4.13, respectively. A coordination number of 3.63 was predicted by the OPLS-AA force field, while the new force field gave a coordination number of 3.37.

## V. Conclusions

A new force field for carboxylic acids was presented that reproduces accurately saturated vapor and liquid densities and critical properties. For acetic acid, the new force field predicts saturated liquid densities that are within 1.6% of experiment. Predictions of the vapor pressure of acetic were less robust, with the new force field overpredicting experimental values by up to 50%. The critical temperature and density were determined and were within 1% of experiment. Comparisons made with the predictions of OPLS-UA, OPLS-AA, and CHARMM force fields show that the new force field is a significant improvement with respect to the prediction of coexistence properties, vapor pressures, and critical properties. The transferability of the force field is demonstrated via simulations of pentanoic and octanoic acid.

Simulations in the isobaric isothermal ensemble were used to investigate the structural properties of acetic acid in the liquid phase. All of the force fields predicted the presence of hydrogen-bonded dimers. The CHARMM and OPLS-UA force fields were found to give the best reproduction of the hydroxyl hydrogen coordination number, while the predictions of the OPLS-AA and new force field were less robust. However, without more detailed experimental data, it is not possible to determine with certainty which of the force fields provides the best representation of the liquid-phase structure. To remedy this, our group has undertaken a combined neutron and X-ray scattering study, which will be presented in a future work.

**Acknowledgment.** The authors would like to thank Bin Chen, Marcus Martin, and Ilja Siepmann for helpful discussions. Financial support from a Minnesota Supercomputing Institute Research Scholarship (J.J.P.) and NSF CTS-0138393 is gratefully acknowledged. Part of the computer resources used in this work were provided by the Minnesota Supercomputing Institute.

## References and Notes

- Lehmle, H. J.; Bummer, P. M. *J. Colloid Interface Sci.* **2002**, *249*, 381.
- Lehmle, H. J.; Jay, M.; Bummer, P. M. *Langmuir* **2000**, *16*, 10161.
- Lehmle, H. J.; Bummer, P. M. *J. Fluorine Chem.* **2002**, *117*, 17.
- Yablon, D. G.; Giancarlo, L. C.; Flynn, G. W. *J. Phys. Chem. B* **2000**, *104*, 7627.
- Chen, B.; Potoff, J. J.; Siepmann, J. I. *J. Phys. Chem. B* **2001**, *105*, 3093.
- Sum, A. K.; Bidy, M. J.; de Pablo, J. J. *J. Phys. Chem. B* **2003**, *107*, 14443.
- Bernal, J. D.; Fowler, R. H. *J. Chem. Phys.* **1993**, *97*, 13841.
- Jorgensen, W. L. *J. Chem. Phys.* **1982**, *77*, 4156.
- Jorgensen, W. L.; Chandrasekhar, J.; Madura, J. D.; Impey, R. W.; Klein, M. L. *J. Phys. Chem.* **1983**, *79*, 926.
- Berendsen, H. J. C.; Grigera, J. R.; Straatsma, T. P. *J. Phys. Chem.* **1987**, *91*, 6261.
- Boulougouris, G. C.; Economou, I. G.; Theodorou, D. N. *J. Phys. Chem. B* **1998**, *102*, 1029.
- Errington, J.; Panagiotopoulos, A. Z. *J. Phys. Chem. B* **1998**, *102*, 7470.
- Chen, B.; Xing, J.; Siepmann, J. I. *J. Phys. Chem. B* **2000**, *104*, 2391.
- Briggs, J. M.; Nguyen, T. B.; Jorgensen, W. L. *J. Phys. Chem.* **1991**, *95*, 3315.
- Jorgensen, W. L.; Maxwell, D. S.; Tirado-Rives, J. *J. Am. Chem. Soc.* **1996**, *118* (45), 11225.
- MacKerell, A. D., Jr.; Winkiewicz-Kuczera, J.; Karplus, M. *J. Am. Chem. Soc.* **1995**, *117*, 11946.
- MacKerell, A. D., Jr.; Basford, D.; Bellot, M.; Dunbrack, J.; Evanseck, J. D.; Field, M. J.; Fischer, S.; Gao, J.; Guo, H.; Ha, S.; Joseph-McCarty, D.; Kuchnin, L.; Kuczera, K.; Lau, F. T. W.; Mattos, C.; Michnick, S.; Ngo, T.; Nguyen, D. T.; Prodhom, B.; Reiher, W. E.; Roux, B.; Schlenkrich, M.; Smith, J. C.; Stote, R.; Strauh, J.; Watannabe, M.; Winkiewicz-Kuczera, J.; Yin, D.; Karplus, M. *J. Phys. Chem. B* **1998**, *102*, 3586.
- Chen, B.; Siepmann, J. I. *J. Phys. Chem. B* **2000**, *104*, 8725.
- Martin, M. G.; Siepmann, J. I. *J. Phys. Chem. B* **1998**, *102*, 2569.
- Potoff, J. J.; Siepmann, J. I. *AIChE J.* **2001**, *47*, 1676.
- Lorentz, H. A. *Ann. Phys.* **1881**, *12*, 127.
- Berthelot, D. C. R. *Hebd. Seanc. Acad. Sci., Paris* **1898**, *126*, 1703.
- Allinger, N. L.; Chang, S. H. M. *Tetrahedron* **1977**, *33*, 1561.
- Jorgensen, W. L.; Madura, J. D.; Swenson, C. J. *J. Am. Chem. Soc.* **1984**, *106*, 6638.
- Frisch, M. J.; Trucks, G. W.; Schlegel, H. B.; Scuseria, G. E.; Robb, M. A.; Cheeseman, J. R.; Zakrzewski, V. G.; Montgomery, J. A.; Stratmann, R. E.; Burant, J. C.; Dapprich, S.; Millam, J. M.; Daniels, A. D.; Kudin, K. N.; Strain, M. C.; Farkas, O.; Tomasi, J.; Barone, V.; Cossi, M.; Cammi, R.; Mennucci, B.; Pomelli, C.; Adamo, C.; Clifford, S.; Ochterski, J.; Petersson, G. A.; Ayala, P. Y.; Cui, Q.; Morokuma, K.; Malick, D. K.; Rabuck, A. D.; Raghavachari, K.; Foresman, J. B.; Cioslowski, J.; Ortiz, J. V.; Stefanov, B. B.; Liu, G.; Liashenko, A.; Piskorz, P.; Komaromi, I.; Gomperts, R.; Martin, R. L.; Fox, D. J.; Keith, T.; Al-Laham, M. A.; Peng, C. Y.; Nanayakkara, A.; Gonzalez, C.; Challacombe, M.; Gill, P. M. W.; Johnson, B. G.; Chen, W.; Wong, M. W.; Andres, J. L.; Head-Gordon, M.; Replogle, E. S.; Pople, J. A. *Gaussian 98*; Gaussian, Inc.: Pittsburgh, PA, 1998.
- Ferrenberg, A. M.; Swendsen, R. H. *Phys. Rev. Lett.* **1988**, *61*, 2635.
- Potoff, J. J.; Panagiotopoulos, A. Z. *J. Chem. Phys.* **1998**, *109*, 10914.
- Esselink, K.; Loyens, L. D. J. C.; Smit, B. *Phys. Rev. E* **1995**, *51*, 1560.
- Martin, M. G.; Siepmann, J. I. *J. Phys. Chem. B* **1999**, *103*, 4508.
- McDonald, I. R. *Mol. Phys.* **1972**, *23*, 41.
- Allen, M. P.; Tildesley, D. J. *Computer Simulation of Liquids*, 1st ed.; Oxford University Press: Oxford, 1987.
- Ferrenberg, A. M.; Swendsen, R. H. *Phys. Rev. Lett.* **1989**, *63*, 1195.
- Panagiotopoulos, A. Z. *Mol. Phys.* **1987**, *61*, 813.
- Panagiotopoulos, A. Z.; Quirke, N.; Stapleton, M.; Tildesley, D. J. *Mol. Phys.* **1988**, *63*, 527.
- Panagiotopoulos, A. Z. *Mol. Simul.* **1992**, *9*, 1.
- Martin, M. G.; Chen, B.; Wick, C.; Stubbs, J. M.; Potoff, J. J.; Siepmann, J. I. *MCCCS-Towhee*, <http://www.cs.sandia.gov/projects/towhee/index.html>.
- Rowlandson, J. S.; Widom, B. *Molecular Theory of Capillarity*; Clarendon Press: Oxford, 1982.
- Rowlinson, J. S.; Swinton, F. L. *Liquids and Liquid Mixtures*, 3rd ed.; Butterworth: London, 1982.
- Wilding, N. B. *Phys. Rev. E* **1995**, *52*, 602.
- Vargaftik, N. B. *Handbook of Physical Properties of Liquids and Gases: Pure Substances and Mixtures*, 2nd ed.; Hemisphere: Bristol, PA, 1983.
- Stoll, J.; Vrabec, J.; Hasse, H.; Fischer, J. *Fluid Phase Equilib.* **2001**, *179*, 339.
- Chen, B.; Siepmann, J. I. *J. Phys. Chem. B* **1999**, *103*, 5370.
- Errington, J. R.; Panagiotopoulos, A. Z. *J. Phys. Chem. B* **1999**, *103*, 6314.
- Nath, S. K.; Escobedo, F. A.; de Pablo, J. J. *J. Chem. Phys.* **1998**, *108*, 9905.
- Ungerer, P.; Beauvais, C.; Delhomme, J.; Boutin, A.; Rousseau, B.; Fuchs, A. H. *J. Chem. Phys.* **2000**, *112*, 5499.
- Jorgensen, W. L. *J. Phys. Chem.* **1986**, *90*, 1276.
- Daubert, T. E.; Danner, R. P. *Physical and Thermodynamic Properties of Pure Chemicals*; Taylor and Francis Inc.: Levittown, PA, 1994.
- Stull, D. *Ind. Eng. Chem.* **1947**, *39*, 517.
- Eckert, C. A.; Pouillot, L. L.; Knutson, B. L.; Gurdial, G. S. *J. Supercrit. Fluids* **1995**, *8*, 1.
- Reid, R. C.; Prausnitz, J. M.; Poling, B. E. *The Properties of Gases and Liquids*; McGraw-Hill: New York, 1988.
- Lydersen, A. L. *Engineering Experimental Station, Report 3*; University of Wisconsin College of Engineering: Madison, WI, April 1955.
- Bertagnolli, H. *Chem. Phys. Lett.* **1982**, *93*, 287.
- Urquidí, J.; Benmore, C.; Potoff, J. J. Unpublished data.